AFRL-RX-WP-JA-2014-0157

DENSITY FUNCTIONAL THEORY BASED GENERALIZED EFFECTIVE FRAGMENT POTENTIAL METHOD (POSTPRINT)

Ruth Pachter
AFRL/RXA

JULY 2014
Interim Report

AIR FORCE RESEARCH LABORATORY
MATERIALS AND MANUFACTURING DIRECTORATE
WRIGHT-PATTERSON AIR FORCE BASE, OH 45433-7750
AIR FORCE MATERIEL COMMAND
UNITED STATES AIR FORCE

NOTICE AND SIGNATURE PAGE

Using Government drawings, specifications, or other data included in this document for any purpose other than Government procurement does not in any way obligate the U.S. Government. The fact that the Government formulated or supplied the drawings, specifications, or other data does not license the holder or any other person or corporation; or convey any rights or permission to manufacture, use, or sell any patented invention that may relate to them.

This report was cleared for public release by the USAF 88th Air Base Wing (88 ABW) Public Affairs Office (PAO) and is available to the general public, including foreign nationals.

Copies may be obtained from the Defense Technical Information Center (DTIC) (http://www.dtic.mil).

AFRL-RX-WP-JA-2014-0157 HAS BEEN REVIEWED AND IS APPROVED FOR PUBLICATION IN ACCORDANCE WITH ASSIGNED DISTRIBUTION STATEMENT.

//Signature//	//Signature//
RUTH PACHTER Senior Scientist Functional Materials Division	TIMOTHY J. BUNNING, Chief Functional Materials Division Materials and Manufacturing Directorate

This report is published in the interest of scientific and technical information exchange, and its publication does not constitute the Government's approval or disapproval of its ideas or findings.

REPORT DOCUMENTATION PAGE

Form Approved
OMB No. 074-0188

1. REPORT DATE (DD-MM-YYYY)	2. REPORT TYPE	3. DATES COVERED *(From – To)*
July 2014	Interim	28 March 2013 – 03 June 2014

4. TITLE AND SUBTITLE
DENSITY FUNCTIONAL THEORY BASED GENERALIZED EFFECTIVE FRAGMENT POTENTIAL METHOD (POSTPRINT)

5a. CONTRACT NUMBER
FA8650-09-D-5430-0025

5b. GRANT NUMBER

5c. PROGRAM ELEMENT NUMBER
62102F

6. AUTHOR(S)
(see back)

5d. PROJECT NUMBER
4347

5e. TASK NUMBER

5f. WORK UNIT NUMBER
X0KU

7. PERFORMING ORGANIZATION NAME(S) AND ADDRESS(ES)
(see back)

8. PERFORMING ORGANIZATION REPORT NUMBER

9. SPONSORING / MONITORING AGENCY NAME(S) AND ADDRESS(ES)
Air Force Research Laboratory
Materials and Manufacturing Directorate
Wright Patterson Air Force Base, OH 45433-7750
Air Force Materiel Command
United States Air Force

10. SPONSOR/MONITOR'S ACRONYM(S)
AFRL/RXA

11. SPONSOR/MONITOR'S REPORT NUMBER(S)
AFRL-RX-WP-JA-2014-0157

12. DISTRIBUTION / AVAILABILITY STATEMENT
Distribution A. Approved for public release; distribution unlimited. This report contains color.

13. SUPPLEMENTARY NOTES
PA Case Number: 88ABW-2014-0839; Clearance Date: 3 March 2014. Journal article published in The Journal of Chemical Physics 140, 244101 (2014). © 2014 AIP Publishing LLC. The U.S. Government is joint author of the work and has the right to use, modify, reproduce, release, perform, display or disclose the work. The final publication is available at http://dx.doi.org/10.1063/1.4883488.

14. ABSTRACT
We present a generalized Kohn-Sham (KS) density functional theory (DFT) based effective fragment potential (EFP2-DFT) method for the treatment of solvent effects. Similar to the original Hartree-Fock (HF) based potential with fitted parameters for water (EFP1) and the generalized HF based potential (EFP2-HF), EFP2-DFT includes electrostatic, exchange-repulsion, polarization, and dispersion potentials, which are generated for a chosen DFT functional for a given isolated molecule. The method does not have fitted parameters, except for implicit parameters within a chosen functional and the dispersion correction to the potential. The electrostatic potential is modeled with a multipolar expansion at each atomic center and bond midpoint using Stone's distributed multipolar analysis. The exchange-repulsion potential between two fragments is composed of the overlap and kinetic energy integrals and the nondiagonal KS matrices in the localized molecular orbital basis. The polarization potential is derived from the static molecular polarizability. The dispersion potential includes the intermolecular D3 dispersion correction of Grimme et al. [J. Chem. Phys. 132, 154104 (2010)]. The potential generated from the CAMB3LYP functional has mean unsigned errors (MUEs) with respect to results from coupled cluster singles, doubles, and perturbative triples with a complete basis set limit (CCSD(T)/CBS) extrapolation, of 1.7, 2.2, 2.0, and 0.5 kcal/mol, for the S22, water-benzene clusters, water clusters, and n-alkane dimers benchmark sets, respectively. The corresponding EFP2-HF errors for the respective benchmarks are 2.41, 3.1, 1.8, and 2.5 kcal/mol. Thus, the new EFP2-DFT-D3 method with the CAMB3LYP functional provides comparable or improved results at lower computational cost and, therefore, extends the range of applicability of EFP2 to larger system sizes.

15. SUBJECT TERMS
chemistry, computational, computer analysis, laser hardening, material development, nanotechnology, physics

16. SECURITY CLASSIFICATION OF:			17. LIMITATION OF ABSTRACT	18. NUMBER OF PAGES	19a. NAME OF RESPONSIBLE PERSON *(Monitor)*
a. REPORT	b. ABSTRACT	c. THIS PAGE			Ruth Pachter
Unclassified	Unclassified	Unclassified	SAR	14	19b. TELEPHONE NUBER *(include area code)* (937) 255-9689

REPORT DOCUMENTATION PAGE Cont'd

6. AUTHOR(S)

Ruth Pachter - Materials and Manufacturing Directorate, Air Force Research Laboratory, Functional Materials Division
Kiet A. Nguyen – UES, Inc.
Paul N. Day – General Dynamics Information Technology, Inc.

7. PERFORMING ORGANIZATION NAME(S) AND ADDRESS(ES)

AFRL/RXA
Air Force Research Laboratory
Materials and Manufacturing Directorate
Wright-Patterson Air Force Base, OH 45433-7750

UES, Inc.
Dayton, OH 45432

General Dynamics Information Technology, Inc.
Dayton, Ohio 45431

Density functional theory based generalized effective fragment potential method

Kiet A. Nguyen,[1,2,a)] Ruth Pachter,[1,a)] and Paul N. Day[1,3]
[1]*Air Force Research Laboratory, Wright-Patterson Air Force Base, Ohio 45433, USA*
[2]*UES, Inc., Dayton, Ohio 45432, USA*
[3]*General Dynamics Information Technology, Inc., Dayton, Ohio 45431, USA*

(Received 30 January 2014; accepted 3 June 2014; published online 23 June 2014)

We present a generalized Kohn-Sham (KS) density functional theory (DFT) based effective fragment potential (EFP2-DFT) method for the treatment of solvent effects. Similar to the original Hartree-Fock (HF) based potential with fitted parameters for water (EFP1) and the generalized HF based potential (EFP2-HF), EFP2-DFT includes electrostatic, exchange-repulsion, polarization, and dispersion potentials, which are generated for a chosen DFT functional for a given isolated molecule. The method does not have fitted parameters, except for implicit parameters within a chosen functional and the dispersion correction to the potential. The electrostatic potential is modeled with a multipolar expansion at each atomic center and bond midpoint using Stone's distributed multipolar analysis. The exchange-repulsion potential between two fragments is composed of the overlap and kinetic energy integrals and the nondiagonal KS matrices in the localized molecular orbital basis. The polarization potential is derived from the static molecular polarizability. The dispersion potential includes the intermolecular D3 dispersion correction of Grimme *et al.* [J. Chem. Phys. **132**, 154104 (2010)]. The potential generated from the CAMB3LYP functional has mean unsigned errors (MUEs) with respect to results from coupled cluster singles, doubles, and perturbative triples with a complete basis set limit (CCSD(T)/CBS) extrapolation, of 1.7, 2.2, 2.0, and 0.5 kcal/mol, for the S22, water-benzene clusters, water clusters, and *n*-alkane dimers benchmark sets, respectively. The corresponding EFP2-HF errors for the respective benchmarks are 2.41, 3.1, 1.8, and 2.5 kcal/mol. Thus, the new EFP2-DFT-D3 method with the CAMB3LYP functional provides comparable or improved results at lower computational cost and, therefore, extends the range of applicability of EFP2 to larger system sizes. © *2014 AIP Publishing LLC*. [http://dx.doi.org/10.1063/1.4883488]

I. INTRODUCTION

Efficient and accurate methods for describing intermolecular interactions are of considerable interest in many fields of chemistry, physics, material, and biological sciences because accurate first principles methods are computationally demanding with increasing system size for materials in solution, such as biological systems, colloidal quantum dots, and other materials in the condensed phase. To reduce the computational cost, the effective fragment potential (EFP) method was developed to explicitly model intermolecular interactions for molecular complexes (e.g., $(H_2O)_n$) by using quantum mechanical (QM) properties of a single molecule.[1–4] The established QM parameters can be stored for future use or reproduced on the fly as needed. Thus, EFP potentials are similar in spirit to molecular mechanics force fields that are generated by using *ab initio* data such as the SIBFA (sum of interactions between fragments *ab initio* computed).[5] In the EFP methods, molecules within a complex are replaced by frozen molecular fragments with fixed internal coordinates. The EFP intermolecular interactions are represented by Coulomb, induction, and dispersion terms that are generated by auxiliary first principles calculations. The present work focuses on the development of a second generation EFP (EFP2) based on density functional theory (DFT). A number of reviews[1–4] have been published, including most recent EFP developments[4] on the interface with the ground and excited state *ab initio* wavefunctions.

The first generation of EFPs[1,3] based on Hartree-Fock (HF) and density functional theory (DFT) were originally formulated and implemented to model water (called EFP1).[3,6,7] The HF based EFP2 extension with dispersion between fragments[8] or HF-EFP2[9] systems is a more general and parameter-free method for *any* molecular species.[8–12] However, the EFP1-DFT[7] potential was fitted using the B3LYP functional, which lacks long-range and dispersion interactions. The EFP1-HF[3] method was fitted to reproduce results for HF, which does not include the important electron correlation effects. The DFT based EFP2 with dispersion interactions offers advantages of DFT over HF at comparable computational cost. However, as the cost for evaluating the dynamic polarizability becomes prohibitive for obtaining the dispersion potential for large EFP2-HF systems, we are motivated to include the simple D3 dispersion potential, which has been recently refined to high accuracy and broad applicability.[13] The geometry based D3 dispersion potential is also compatible with the DFT-EFP2 dispersion interaction. The dispersion interactions for QM systems with EFP for HF-EFP2 practically require a separated treatment for the QM part calculated with

[a)]Authors to whom correspondence should be addressed. Electronic addresses: kiet.nguyen@wpafb.af.mil and ruth.pachter@wpafb.af.mil.

dipole integrals and orbital energies.[9] In this work, we implemented and evaluated the accuracy of the DFT-EFP2 potential, using the mean unsigned errors (MUE) and mean signed errors (MSE), relative to a number of benchmarks from the coupled cluster (CC) method with singles, doubles (CCSD) and noniterative triples with the extrapolation to the complete basis set limit (CCSD(T)/CBS).[14–18]

The paper is organized as follows. After providing a description of the method (Sec. II) and computational details (Sec. III), we present results and discussion for the benchmarking (Sec. IV). Section V provides a summary of our results and conclusions for the paper.

II. THEORY

Considering a complex with two or more non-bonded interacting molecules (fragments), the quantity of interest is its total interaction energy. The EFP methods for obtaining the interaction energy have been described in previous papers.[1,3,7,8] Therefore, we only briefly review the theory in order to document our implementation of the EFP2-DFT method with the D3[13] dispersion potential. The EFP2 potential with electrostatic Coulomb (V_k^{elec}), polarization (V_l^{pol}), exchange-repulsion (V_m^{Ex}), and dispersion (V^{Disp}) contributions from an s fragment can be written as

$$V_{\text{EFP2}}(s,\mathbf{r}) = \sum_{k=1}^{K} V_k^{\text{Elec}}(s,\mathbf{r}) + \sum_{l=1}^{L} V_l^{\text{Pol}}(s,\mathbf{r}) + \sum_{m=1}^{M} V_m^{\text{Ex}}(s,\mathbf{r}) + V^{\text{Disp}}(s,\mathbf{r}), \quad (1)$$

where each fragment indexed by s could have a number (K, L, M) of expansion points; $\mathbf{r}$ is the electronic coordinate. The V_k^{elec} term describes classical electrostatic interactions between the charge distributions of the effective fragments. The electrostatic energy can be effectively represented by distributed multipoles at large intermolecular distance while the charge overlap of the fragment's electron clouds at the short-range is also taken into account as given in Subsection II A. The non–classical exchange–repulsion V_m^{Ex} energy arising from electron exchange, which requires a QM treatment (Subsection II B). The polarization V_l^{pol} term arises from the mutual perturbation of electrostatic fields of the unperturbed fragments. The EFP polarization potential is approximated by using polarizability tensors as described in Subsection II C. The dispersion V^{Disp} term originates from induced dipole-dipole interactions at the lowest order, which is treated using dynamic polarizabilities. The treatment of dispersion for EFP is described in Subsection II D.

A. Electrostatic potential

The electrostatic potential consists of a multicenter distributed multipolar expansion (DMA), carried out with the charge (q), dipole (μ), quadrupole (Θ), and octopole (Ω) moments as[7]

$$V_k^{\text{Elec}}(s,\boldsymbol{r}) = \frac{q_k(s)q_r}{r_{rk}} - \sum_{\alpha}^{x,y,z} \mu_\alpha^k(s) f_\alpha(r_{rk}) - \frac{1}{3}\sum_{\alpha,\beta}^{x,y,z} \Theta_{\alpha\beta}^k(s) f_{\alpha\beta}(r_{rk}) - \frac{1}{15}\sum_{\alpha,\beta}^{x,y,z} \Omega_{\alpha\beta\gamma}^k(s) f_{\alpha\beta\gamma}(r_{rk}), \quad (2)$$

where $f_\alpha, f_{\alpha\beta}$, and $f_{\alpha\beta\gamma}$ are the QM electric field, field gradient, and field Hessian, respectively.

The multipolar expansion at each atomic center and bond midpoint are done with Stone's distributed multipolar analysis using Kohn-Sham (KS) density.[19] As distributed multipolar expansion of a molecular electrostatic potential is only well represented at large intermolecular distances, the point charge model of Eq. (2) must account for overlapping charge densities by a distance-dependent cutoff function.[3,20,21] The nuclei of a molecule are not shielded by their own electron density, leading to a greater attraction for electron density associated with other molecules. This effect is estimated by an exponential damping function fit to the quantum mechanical electrostatic potential over a grid points.[21]

B. Exchange-repulsion potential

The exchange energy arises from the Pauli exclusion principle for electrons with like spin, which requires the wavefunctions to be antisymetric with respect to electron exchange. The exchange-repulsion potential is obtained by subtracting the classical Coulomb energy from the first-order intermolecular interaction energy from symmetry adapted perturbation theory,[22] which is identical to the Heitler-London energy.[1] By neglecting the internal energy and truncating the intermolecular overlap expansion after second order, the approximated exchange-repulsion potential between two EFP fragments (A and B) can be separated into three terms:[11]

$$V^{\text{Ex}} = V^{\text{Ex}}(S^0) + V^{\text{Ex}}(S^1) + V^{\text{Ex}}(S^2). \quad (3)$$

The zeroth order term is approximated as

$$V^{\text{Ex}}(S^0) = -2\sum\nolimits_{i\in\text{A}}\sum\nolimits_{j\in\text{B}} \langle i|K_j|i\rangle, \quad (4)$$

where K_j is the electron exchange operator. Using the spherical Gaussian overlap (SGO) approximation,[11] the zeroth order intermolecular exchange energy for RHF becomes

$$V^{\text{Ex}}(S^0) = -2\sum_{i\in\text{A}}\sum_{j\in\text{B}} 2\sqrt{\frac{-2\ln S_{ij}}{\pi}}\frac{(S_{ij})^2}{R_{ij}}, \quad (5)$$

where S_{ij} is the overlap integral of the localized molecular orbitals (LMOs) and R_{ij} is the distance between LMO centroids. The first order term is approximated as

$$V^{\text{Ex}}(S^1) - 2\sum_{i\in\text{A}}\sum_{j\in\text{B}} S_{ij}\Big[V_{ij,A} + V_{ij,B} + \sum_{k\in\text{A}}\langle i\,|2J_k - K_k|\,j\rangle + \sum_{l\in\text{B}}\langle i\,|2J_l - K_l|\,j\rangle\Big], \quad (6)$$

where J_k is the Coulomb operator, K_k is the exchange operator, and $V_{ij,\mathrm{A}}$ is the potential due to nuclei in A. For a RHF wavefunction the first order term can be written in terms of the Fock matrixes, overlap integrals (S), and kinetic energy integrals (T) of the LMOs as

$$V^{\mathrm{Ex}}(S^1) = -2\sum_{i\in\mathrm{A}}\sum_{j\in\mathrm{B}} S_{ij}\left[\sum_{k}^{\mathrm{A}} F^{\mathrm{A}}_{ik}S_{kj} + \sum_{l}^{\mathrm{B}} F^{\mathrm{B}}_{jl}S_{li} - 2T_{ij}\right]. \tag{7}$$

For DFT based EFP2, F is the nondiagonal KS matrix in the LMO basis, instead of the Fock matrix. The second order term for the exchange-repulsion potential is approximated as

$$\begin{aligned} V^{\mathrm{EX}}(S^2) = 2\sum_{i\in\mathrm{A}}\sum_{j\in\mathrm{B}} S_{ij}\Bigg[&\sum_{k\in\mathrm{A}} S_{kj}\left(V_{ik,B} + \sum_{l\in\mathrm{A}}\langle i\,|2J_k|\,k\rangle\right) \\ &+ \sum_{l\in\mathrm{B}} S_{kj}\left(V_{il,A} + \sum_{k\in\mathrm{A}}\langle j\,|2J_k|\,l\rangle\right) \\ &+ \sum_{l\in\mathrm{B}} S_{il}\left(V_{jl,A} + \sum_{k\in\mathrm{A}}\langle j\,|2J_k|\,l\rangle\right) \\ &- \sum_{K\in\mathrm{A}}\sum_{l\in\mathrm{B}} |S_{kl}\ \langle ik\,|lj|\rangle\Bigg]. \end{aligned} \tag{8}$$

The integrals in $V^{\mathrm{Ex}}\left(S^2\right)$ are modeled with classical electrostatics for both RHF and DFT as

$$\begin{aligned} V^{\mathrm{Ex}}(S^2) \approx 2\sum_{i\in\mathrm{A}}\sum_{j\in\mathrm{B}} (S_{ij})^2\left[\sum_{J\in\mathrm{B}} -\frac{Z_J}{R_{iJ}} + 2\sum_{l\in\mathrm{B}} -\frac{1}{R_{il}}\right] \\ + \sum_{I\in\mathrm{A}} -\frac{Z_J}{R_{Ij}} + 2\sum_{k\in\mathrm{A}}\frac{1}{R_{kj}} - \frac{1}{R_{ij}}. \end{aligned} \tag{9}$$

The indexes i, k and j, l run over the LMOs of fragment A and B, respectively. R_{iJ} is the distance between LMO centroid i and the nucleus J. The choice of DFT functionals affects the accuracy of EFP exchange repulsion potential (Eqs. (3)–(9)) that includes the HF exchange (for hybrid functionals) and KS matrices. Although DFT functionals using the generalized gradient approximation (GGA) provide reasonable energetics for some weakly bound systems, GGA potentials exhibit an exponential decay in the asymptotic regions of molecular systems, instead of the correct $-1/r$ decay, leading to large errors for intermolecular binding energies.[23–25] Hybrid functionals that include a small fraction of the exact HF exchange deliver more accurate results for thermochemistry. However, these potentials decay as $-c/r$ (where c is fraction or scaling factor of HF exchange), not the correct $-1/r$ decay. Long-range corrected (LC) or Coulomb attenuated (CA) hybrids significantly reduce of the self-interaction errors associated with hybrid functionals by retaining the full HF exchange only for long-range electron-electron interactions in the asymptotic regions.[26] Thus, hybrid, LC, or CA functionals represent an appropriate choice. The CAMB3LYP[27] functional with available dispersion parameters[28] is, therefore, chosen for the present work. To ensure correct long-range interactions, the SGO integrals (Eq. (5)) are not scaled in DFT based EFP2.

C. Polarization potential

The polarization potential is calculated as

$$V_l^{\mathrm{Pol}} = \sum_{\alpha,\beta}^{x,y,z} f_\alpha(\mathrm{r}_l)\,\alpha^l_{\alpha\beta}(s)\,\langle f_\beta(\mathrm{r}_l)\rangle, \tag{10}$$

where f is the field generated by QM system and fragments. The polarizability $\alpha^l_{\alpha\beta}$ for a LMO ϕ^0_i by can be obtained by the finite-field method as[29]

$$\alpha^i_{rs} = \frac{\mu^i_s}{F_r}, \tag{11}$$

where μ^i_s is the s component of the dipole moment induced by an electric field applied along direction r, F_r,

$$\mu^i_s = -2\left[\langle\phi'_i|r_s|\phi'_i\rangle - \langle\phi^0_i|r_s|\phi^0_i\rangle\right]. \tag{12}$$

The induced dipole (Eq. (12)) is assumed to be a linear function of the applied field. However, for the nonuniform fields encountered in molecular interactions for systems with more than one fragment, the induced moments within each fragment depend on the electric fields of the other fragment as well as the active part of the QM part of the system, and the fragment–fragment polarization energy must be iterated to self-consistency. An induced dipole is placed at the centroid r_s of each LMO in the valence shell. For example in methane, the LMO centroid locations occur along the four C–H bonds axes. Note that different LMOs result in different sets of polarizability tensors. LMO centroid positions that are not well determined in certain cases of high symmetry and for some aromatic systems, lead to unphysically large components of the polarizability tensors. To obtain the complete polarizability matrix, at least three applied Cartesian (x, y, z) fields SCF calculations must be carried out, in addition to the zero-field SCF calculations. The SCF convergence of 10^{-10} (about 2 orders of magnitude tighter than is acceptable for other applications) leads to induced dipole moments within 10^{-6} to 10^{-7} au of the precise values. Thus, the applied field of 10^{-4} au leads to an uncertainty of 10^{-2} to 10^{-3} for the polarizability using the equations above. In the cases in which the finite-field method described above resulted in unphysically large components of the polarizability, analytical methods have been developed using coupled perturbed Hartree-Fock (CPHF) equations[30] with exact[31–33] and approximate[34] (A-CPHF) response vectors. The approximate response vectors include only HF orbital energies and dipole moments. Thus, the coupled perturbed Kohn-Sham (CPKS)[35,36] equations with approximate (A-CPKS) response vectors that include KS orbital energies and dipole moments, are in analogy to the A-CPHF equations.[34]

In the EFP2 model, the polarization potential (Eq. (10)) currently includes only dipole polarizabilities. The method, in principle, can be extended to any order of polarization but with at the added cost and complexity of analytical gradients of polarization energy with respect to translation and rotation motions of the fragments. However, benchmarks of symmetry-adapted perturbation theory calculations indicated that the main source of EFP2 errors come from the underestimation of the Coulomb and polarization terms that are

partially compensated by the underestimation of the exchange repulsion term.[37]

D. Dispersion potential

Calculations of the dispersion potential for EFP2-HF were done using anisotropic dynamic polarizability tensors evaluated over imaginary frequencies for the C_6 term while higher order terms were estimated as 1/3 of the C_6 term. The method has been described in detail previously.[8,9] The D3 dispersion potential is calculated as[13,28]

$$V^{\mathrm{Dis}} = \sum_{AB} \sum_{n=6,8,..} s_n \frac{C_n^{AB}}{r_{AB}^n} f_{d,n}\left(\mathrm{r}_{AB}\right), \tag{13}$$

where C_n^{AB} are averaged isotropic dispersion coefficients for AB atomic pairs, r_{AB} is the internuclear distance. Thus, intramolecular dispersion interactions are not included for the fragments. The scaling factors s_n are included for $n > 6$ to ensure asymptotic exactness when C_n^{AB} are exact. The damping functions $f_{d,n}$ for determining the range of the dispersion correction is given as

$$f_{d,n} = \frac{1}{1 + 6\left(\frac{\mathrm{r}_{AB}}{R_0^{AB} S_{r,n}}\right)^{-\alpha_n}}, \tag{14}$$

where $S_{r,n}$ is the adjustable order-dependent scaling parameter of the cutoff radii, R_0^{AB}. In DFT-D3, $S_{r,8}$ is set to unity while $S_{r,6}$ is fitted for a given functional. The α_n parameters (of 14) are global constants.[22,25]

III. COMPUTATIONAL DETAILS

Electronic structure calculations were done using the aug-cc-pVTZ[38,39] basis set. For selected cases, calculations were carried out using the larger correlation-consistent valence quadruple-ζ (aug-cc-pVQZ) basis sets. Kohn-Sham[40] CAMB3LYP calculations were carried out as previously

TABLE I. HF and DFT based EFP2 binding energies (in kcal/mol) for S22 benchmark set.

Systems	Ref.[a]	EFP2-HF[b]	EFP2-DFT-D3[c]	DFT-D3[d]
Hydrogen bonded complexes				
1, $(NH_3)_2$	− 3.15	− 0.52	− 0.38	− 3.43
2, $(H_2O)_2$	− 5.07	− 5.30	− 4.97	− 5.72
3, (Formic acid)$_2$	− 18.81	− 12.92	− 13.16	− 21.13
4, (Formamide)$_2$	− 16.11	− 15.43	− 13.44	− 17.51
5, (Uracil)$_2$	− 20.69	− 20.23	− 20.51	− 22.27
6, 2-Pyridoxine · 2-aminopyridine	− 17.00	− 20.92	− 15.74	− 18.21
7, Adenine · thymine	− 16.74	− 19.22	− 17.28	− 17.75
MUE		2.33	1.88	1.21
Predominantly dispersion complexes				
8, $(CH_4)_2$	− 0.53	− 1.48	− 0.84	− 0.48
9, $(C_2H_4)_2$	− 1.48	− 3.45	− 2.02	− 1.73
10, $C_6H_6 \cdot CH_4$	− 1.45	− 1.87	− 2.49	− 1.59
11, $(C_6H_6)_2$ stack	− 2.62	3.24	2.77	− 2.06
12, (Pyrazine)$_2$	− 4.20	1.35	− 1.75	− 3.65
13, (Uracil)$_2$ stack	− 9.74	− 11.98	− 6.74	− 10.85
14, Indole · benzene stack	− 4.59	7.70	− 1.39	− 3.44
15, Adenine · thymine stack	− 11.66	− 12.15	− 11.10	− 11.14
MUE		3.72	2.06	0.48
Mixed complexes				
16, Ethene · ethine (C_{2v})	− 1.50	− 1.63	− 1.68	− 1.83
17, Benzene · H_2O (C_s)	− 3.29	− 2.61	− 3.59	− 3.51
18, Benzene · NH_3 (C_s)	− 2.32	0.43	0.56	− 2.43
19, Benzene · HCN (C_s)	− 4.55	− 5.71	− 6.31	− 5.05
20, $(C_6H_6)_2$ T−shape	− 2.71	− 3.58	− 2.51	− 2.82
21, Indole · benzene T−shape	− 5.62	− 4.24	− 5.98	− 5.51
22, (Phenol)$_2$	− 7.09	− 7.11	− 5.82	− 7.66
MUE		1.00	0.99	0.28
MUE (22)		2.41	1.66	0.65

[a]References 14 and 16.
[b]EFP2-HF generated with the aug-cc-pVTZ basis set using Edmiston-Ruedenberg localized orbital; MUE of 2.06 kcal/mol (0.9 kcal/mol after geometry optimization) for EFP2-HF using the 6-31+G* basis set for electrostatic and 6-31++G(3df,2p) basis set for other terms. EFP2-HF generated with the 6-311++G(3df,2p) basis set at the MP2/aug-cc-pVTZ geometries: −5.1 kcal/mol (2, water dimer), −2.4 kcal/mol (11, stacked benzene dimer), −3.9 kcal/mol (17, benzene-water), −2.9 kcal/mol (20, T−shape benzene dimer).
[c]Generated with CAMB3LYP/aug-cc-pVQZ using Boys localized orbitals and D3 dispersion correction. Polarization terms for formic acid, uracil, 2-pyridoxine, 2-aminopyridine thymine, indole, C_6H_6, pyrazine, HCN were generated with CAMB3LYP/aug-cc-pVTZ.
[d]CAMB3LYP-D3/aug-cc-pVTZ.

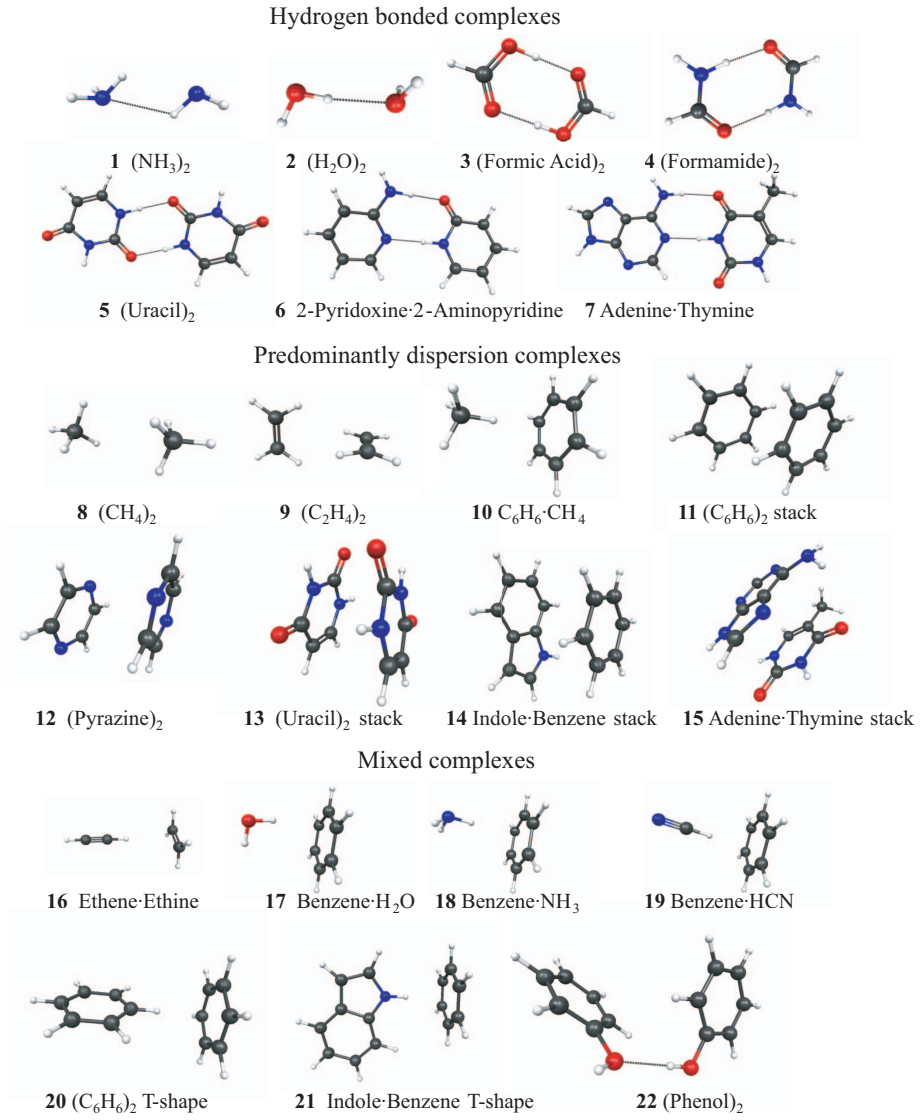

FIG. 1. Structures of S22 data set.

described.[41] Polarizability tensors for all DFT based polarization potentials were obtained using The finite-field method, except for 2-Pyridoxine. Due to unphysically large polarizability tensors obtained with the finite-field method for 2-Pyridoxine, its $\alpha^{I}_{\alpha\beta}$ tensors were obtained using the CPKS method with approximate response vectors that include KS orbital energies and dipole moments.[34]

The S22[14,16] benchmark set reference data were obtained by CCSD(T)/CBS for complexes of common molecules with typical noncovalent interactions. The water-benzene clusters[17] and WATER27[11] reference values were also obtained at the CCSD(T)/CBS level, except for the clusters with n = 20,[42] where MP2/CBS was used. The *n*-alkane dimers[18] benchmark values were CCSD(T)/CBS for ethane to butane and a linear extrapolation method for longer *n*–alkanes. The structures of ethane to heptane were obtained at the MP2/6-31G(d) level.[18] The geometries of *n*–alkane dimers were obtained at MP2/6-311G(d,p) level with fixed geometries of the monomers.[18] All calculations were done using a locally modified version of the GAMESS[43] program.

IV. RESULTS AND DISCUSSION

A. S22 benchmark

The S22 benchmark in Table I includes results for 22 typical complexes (Figure 1) that can be divided into three subsets, hydrogen bonded complexes, predominantly dispersion complexes, and mixed complexes with electrostatic and dispersion interactions. The performance of different EFP2 models for binding energies in the S22 set are given along with the results for the CAMB3LYP functional reported by Goerigk and Grimme.[28] The overall MUEs for 22 typical noncovalent complexes are given along with the MUEs for three subsets. We first discuss the overall performance of binding energies and then consider specific complexes. An overall MUE of 2.41 kcal/mol was obtained using EFP2-HF with the aug-cc-pVTZ basis set. This is comparable with the MUE of 2.06 kcal/mol for EFP2-HF using the 6-31+G* basis set for electrostatics and 6–31++G(3df,2p) basis set for other terms (EFP2-HF-MX). The MUE for EFP2-HF-MX was reduced to 0.9 kcal/mol after geometry optimization. For the DFT based

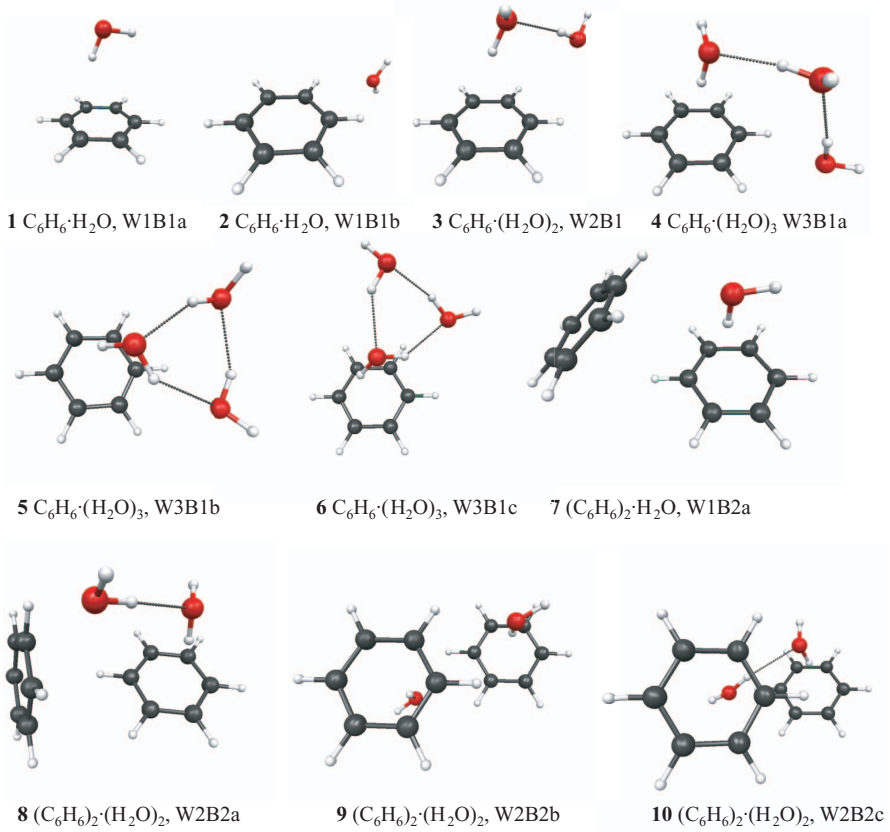

FIG. 2. Structures of water-benzene clusters.

EFP2 method, the MUE of 1.66 kcal/mol is obtained for a potential generated by CAMB3LYP/aug-cc-pVQZ with Boys localized orbitals and the dispersion correction using the D3 ($S_{r,6} = 1.217$, $s_6 = 1.0$, $s_8 = 1.378$) parameters[28] (EFP2-CAMB3LYP-D3). A MUE of 0.98 kcal/mol is obtained with EFP2-CAMB3LYP-D3 after geometry optimization. The D3 attractive dispersion[28] contributions to the binding energies depend on the type of complex and are smaller than the corresponding HF values (see Tables 1S and 2S in the supplementary material[44]). The errors for EFP2-CAMB3LYP-D3 are comparable to those of EFP2-HF-MX. However, the D3 dispersion corrections were obtained at a significantly reduced computational cost in comparison to the coupled perturbed HF method (CPHF) for obtaining dispersion coefficients, expressed in terms of the dynamic polarizabilties over the imaginary frequency range,[8] which is currently used for EFP2-HF. The EFP2 errors are higher than the reported[28] MUE of 0.67 kcal/mol for the D3 correction of CAMB3LYP/def2-QZVP (MUE of 2.52 kcal/mol) using the RI-JK approximation. This is quite small but larger than MUE for the lowest BLYP-D3 (0.23 kcal/mol)[13] functional. The MUE of 0.65 kcal/mol is obtained for CAMB3LYP-D3/aug-cc-pVTZ without using the RI-JK approximation.

B. Water-benzene benchmark

In this section, we examine the water-benzene clusters (Figure 2) and related complexes. A number of complexes (water dimer, benzene dimers, water-benzene) in the S22 set have been considered using EFP2-HF with the 6-311++G(3df,2p) basis set and MP2/aug-cc-pVTZ geometry.[17] The reported[17] EFP2-HF optimized water dimer classical binding energy of 5.1 kcal/mol is in good agreement with our computed EFP2-HF (−5.3 kcal/mol) and EFP2-CAMB3LYP-D3 (−4.97 kcal/mol) values (Table I). For the lowest T–shape structure of the benzene dimer, we obtain a binding energy (without zero–point correction, Table I) of −2.51 (−3.6 kcal/mol) EFP2-CAM-D3

TABLE II. HF and DFT based EFP2 binding energies (in kcal/mol) for the water-benzene clusters benchmark set.

Systems	Ref.[a]	EFP2-HF[b]	EFP2-HF[c]	EFP2-DFT-D3[c]
1, W1B1a	− 3.0	− 3.5	− 3.9	− 2.7
2, W1B1b	− 1.1	− 2.8	− 2.6	− 3.2
3, W2B1	− 8.9	− 10.7	− 10.9	− 9.5
4, W3B1a	− 16.0	− 21.0	− 20.7	− 19.9
5, W3B1b	− 17.3	− 20.9	− 19.6	− 19.5
6, W3B1c	− 16.7	− 20.4	− 19.4	− 18.9
7, W1B2a	− 7.0	− 8.4	− 8.8	− 8.0
8, W2B2a	− 13.0	− 16.7	− 17.3	− 16.0
9, W2B2b	− 10.1	− 17.0	− 16.0	− 15.8
10, W2B2c	− 11.4	− 13.8	− 14.7	− 12.5
MUE		3.1	2.9	2.2

[a]Reference 17.
[b]Generated with the aug-cc-pVQZ basis set at the MP2/cc–pVTZ geometries.
[c]Generated with the 6-311++G(3df,2p) basis set at the MP2/aug-cc-pVTZ geometries.[17]
[d]Generated with CAMB3LYP/aug-cc-pVQZ (CAMB3LYP/aug-cc-pVTZ for polarization potential) using Boys localized orbitals and D3 dispersion correction.

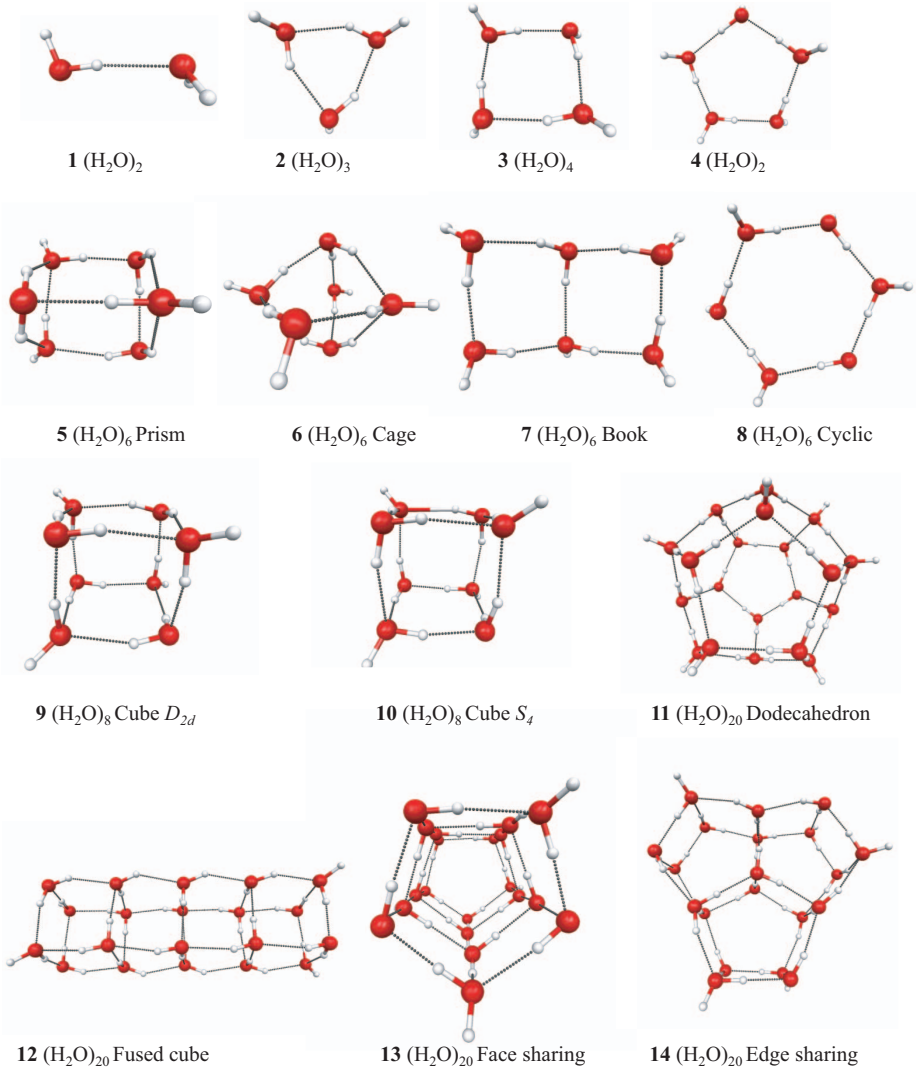

FIG. 3. Structures of water clusters.

(EFP2-HF). EFP2-CAM-D3 predicts the stacked structure to be unbound at the S22 benchmark geometry. However, the EFP2-CAM-D3 (EFP2-HF) binding energies of −2.2 kcal/mol (−1.9 kcal/mol) and −2.8 kcal/mol (−4.0 kcal/mol) were obtained after geometry optimization for the stacked and T-shape dimers, respectively. These values are in good agreement with the previously reported EFP2-HF values of −2.4 kcal/mol (stacked) and −2.9 kcal/mol (T–shape).[17] For benzene-water dimer, the lowest EFP2-HF classical binding energy of −3.9 kcal/mol was reported for the geometry with water on top of the benzene ring.[17] Our computed EFP2-HF values of −2.6 kcal/mol (Table I) and −3.5 kcal/mol (Table II) were obtained at the MP2/cc-pVTZ structure in the S22 benchmark and at the optimized EFP2 geometry,[17] respectively. The corresponding EFP2-CAMB3LYP–D3 values are −3.6 kcal/mol (Table I) and −2.7 kcal/mol (Table II). For complexes with multiple water and benzene molecules, their binding energies are generally overestimated by both the HF and DFT based EFP2 methods. Overall, MUE of about 3 kcal/mol and 2 kcal/mol are obtained with EFP2-HF and EFP2-CAMB3LYP-D3 (Table II).

C. Water clusters

In this validation set, we considered the 14 neutral $(H_2O)_n$ (Figure 3) in the so-called WATER27 benchmark. The benchmark set provides a rigorous test for hydrogen bonding in small $(H_2O)_2$, mid-size $(H_2O)_n$, and the large size of the clusters up to n = 20. The MUEs for HF and DFT based

TABLE III. MUEs for binding energies (in kcal/mol) for the 14 neutral water clusters in the WATER27 benchmark set using EFP2 and other methods.[a]

Basis set/localization method	Edmiston-Ruedenberg	Boys	Pipek-Mezey
EFP2-CAMB3LYP-D3			
aug-cc-pVTZ	5.8	9.8	7.3
aug-cc-pVQZ	7.1	2.0	15.3
EFP2-HF			
aug-cc-pVTZ	10.5	4.7	33.7
aug-cc-pVQZ	1.8	11.0	39.5

[a]MUEs for other methods: 11.8 kcal/mol (EFP1-HF), 43.9 kcal/mol (EFP1-DFT), 13.2 kcal/mol (EFP2-HF using the 6-31+G* basis set for electrostatic with an overlap based damping correction and 6-31++G(3df,2p) basis set for other terms, 20.1 kcal/mol (POL5P), 6.3 kcal/mol, 6.3 kcal/mol (TIP5P), 5.7 (TIP5PE), 4.2 kcal/mol (SPC), 3.3 kcal/mol (SPCE), 1.9 kcal/mol (TIP3P), 1.6 kcal/mol (AMOEBA).

TABLE IV. EFP2 binding energies (in kcal/mol) generated by HF and CAMB3LYP with the aug-cc-pVQZ basis set using Edmiston-Ruedenberg and Boys localized orbitals, respectively, for neutral water clusters in the WATER27 benchmark set compared with other methods.

		PW6B95[b]		EFP1[c]		EFP2	EFP2
Systems	Ref.[a]	KS	D3	HF	DFT	HF	CAMB3LYP
1, $(H_2O)_2$	− 5.0	− 4.7	− 5.0	− 5.0	− 7.7	− 4.9	− 5.0
2, $(H_2O)_3$ cyclic	− 15.8	− 14.7	− 15.7	− 13.6	− 22.1	− 15.9	− 15.6
3, $(H_2O)_4$ cyclic	− 27.4	− 25.8	− 27.3	− 24.1	− 39.7	− 26.7	− 25.6
4, $(H_2O)_5$ cyclic	− 35.9	− 34.0	− 36.0	− 31.8	− 52.8	− 35.5	− 36.5
5, $(H_2O)_6$ prism	− 46.0	− 42.0	− 45.9	− 40.9	− 68.7	− 45.9	− 45.1
6, $(H_2O)_6$ cage	− 45.8	− 42.1	− 45.6	− 40.2	− 68.3	− 45.4	− 45.6
7, $(H_2O)_6$ book	− 45.3	− 42.2	− 45.2	− 40.2	− 67.3	− 44.5	− 43.5
8, $(H_2O)_6$ cyclic	− 44.3	− 42.2	− 44.6	− 39.7	− 65.2	− 43.5	− 45.7
9, $(H_2O)_8$ cube (D_{2d})	− 72.6	− 66.0	− 71.6	− 64.1	− 109.3	− 71.3	− 69.9
10, $(H_2O)_8$ cube (S_4)	− 72.6	− 65.9	− 71.6	− 64.1	− 109.2	− 71.3	− 70.5
11, $(H_2O)_{20}$ dodecahedron	− 200.1	− 182.4	− 197.6	− 176.8	− 301.6	− 197.5	− 203.5
12, $(H_2O)_{20}$ fused cubes	− 212.6	− 184.5	− 203.6	− 182.6	− 318.5	− 208.3	− 207.7
13, $(H_2O)_{20}$ face−sharing	− 215.0	− 185.5	− 204.3	− 183.6	− 320.2	− 211.2	− 212.4
14, $(H_2O)_{20}$ edge−sharing	− 217.9	− 187.8	− 206.2	− 184.8	− 320.7	− 208.8	− 211.9
MUE		9.8	2.6	11.8	43.9	1.8	2.0

[a]Reference 15.
[b]Reference 13.
[c]EFP1-HF results using HF/DH(d,p)//HF/DH(d,p): −42.4 (5, prism), −41.9 (6, cage), −41.5 (7, book), −41.1 (8, cyclic), −66.3 (9, D_{2d} cube), −66.3 (10, S_4 cube).[45]

EFP2 potentials using different localized orbitals and basis sets (aug-cc-pVXZ, X = T, Q) are listed in Table III, along with the errors obtained with other methods. For a given basis set, the variations of the results among different localization schemes can be attributed to the polarization potential (Eq. (10)), that is expanded in terms of LMO polarizability tensors. Although polarization energies obtained with LMO polarizabilities were found to be more accurate than the energies expanded with polarizabilties at the center of mass,[3] different LMOs result in different polarizability tensors and resulting energies. Similarly, the dispersion potential obtained with LMO dynamic polarizabilities,[8] is an additional contributing factor of the deviations for the HF based EFP2. Since both static and dynamic polarizabilities are basis set sensitive, the resulting energies are basis dependent.

The errors for water clusters are generally improved upon going from the aug-cc-pVTZ to aug-cc-pVQZ basis set, except for values obtained with the Pipek-Mezey localized orbitals and the Boys localized orbitals for EFP2-HF. The lowest MUEs of 1.8 kcal/mol and 2.0 kcal/mol were obtained with the Edminston-Ruedenberg and Boys localized aug-cc-pVQZ orbitals for HF and CAMB3LYP based EFP2 potentials, respectively. These errors compare well to the best estimates from DFT-D3 (2.6 kcal/mol for PW6B95, see Table IV) and other (1.6 kcal/mol for AMOEBA) potentials. The binding energies for EFP2 obtained with HF and the CAMB3LYP functional are listed in Table IV along with the results for EFP1, PW6B95 functional, and reference values. We obtain a value of 11.8 kcal/mol for EFP1-HF, which has been applied to study $(H_2O)_n$ for n = 6–20.[45] The MUE (10.5 kcal/mol, see Table III) for a EFP2-HF potential using the aug-cc-pVTZ basis set and Edminston-Ruedenberg localized orbitals is slightly reduced and is comparable to the error (9.8 kcal/mol, see Table IV) for PW6B95 without dispersion corrections. With the D3 dispersion correction, the MUE for PW6B95 reduces to 2.6 kcal/mol. EFP2-CAM-D3 delivers outstanding improvements over EFP2-CPHF and EFP1 fitted potentials obtained for the water clusters benchmark set. The MUE of 2.0 kcal/mol for EFP2-CAMB3LYP is smaller than the corresponding value (2.6 kcal/mol) obtained for the most accurate PW6B95-D3 functional in the WATER27 benchmark set. These errors are quite small, considering the average binding energy of −89.7 kcal/mol. The poor EFP1-B3LYP results might be due to known deficiencies of DFT densities at large interatomic distances in complexes for functionals with asymptotically incorrect exchange-correlation potentials.[25,46]

The ability to predict relative energies of low-energy isomers is important. Thus, we examine the performance of different models for relative stability of $(H_2O)_6$ and $(H_2O)_{20}$ conformers. For $(H_2O)_6$, CCSD(T) gives the following energy ordering for the four isomers: prism < cage < book < cyclic

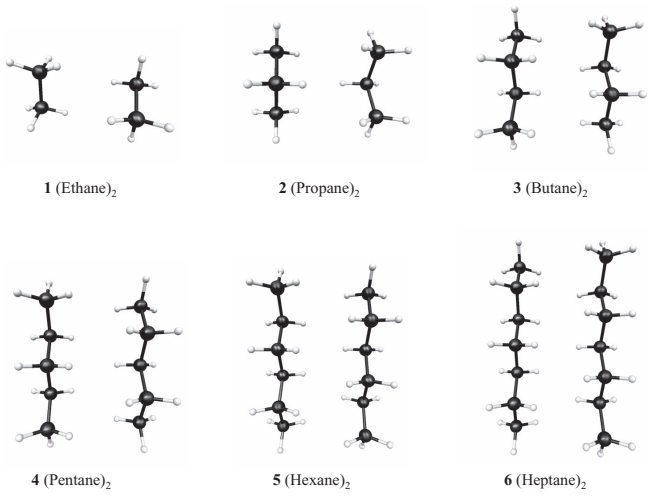

FIG. 4. Structures of *n*-alkane dimers.

TABLE V. HF and DFT based EFP2 binding energies (in kcal/mol) using the aug-cc-pVTZ basis set for the *n*-alkane dimers. Values in parentheses are obtained using the aug-cc-pVQZ basis set.

Systems	Ref.[a]	EFP2-HF[b]	EFP2-DFT-D3[c]
1, Ethane	− 1.22	− 0.16 (−0.28)	− 0.55 (−0.70)
2, Propane	− 1.87	− 2.51 (−2.43)	− 2.27 (−2.20)
3, Butane	− 2.74	− 5.21	− 3.33 (−3.41)
4, Pentane	− 3.80	− 6.28	− 4.21
5, Hexane	− 4.66	− 8.66	− 5.32
6, Heptane	− 5.52	− 9.95	− 5.66
MUE		2.51	0.48

[a]Reference 18.
[b]Generated with the aug-cc-pVTZ basis set at the MP2/cc–pVTZ geometries using Edmiston-Ruedenberg localized orbitals.
[c]Generated with CAMB3LYP/aug-cc-pVTZ using Boys localized orbitals and D3 dispersion correction.

(**5**–**8** in Figure 3). The EFP1 and EFP2-HF models correctly predict the ordering. However, EFP1-DFT excessively overestimates the binding energies while EFP1-HF underestimates the energies. EFP2-CAMB3LYP-D3 predicts small energy gaps among the isomers. For $(H_2O)_{20}$, the reference binding energies predicted by MP2/CBS[42] are available for the stable isomers of the four different topologies. EFP2 models predict the face-sharing instead of the edge-sharing pentagonal prisms as the lowest energy isomer. EFP2-CAMB3LYP-D3 and EFP2-HF models underestimate the binding energies of the lowest energy $(H_2O)_{20}$ isomer by 6.0 kcal/mol and 9.1 kcal/mol, respectively.

D. *n*-Alkane dimers benchmark

The *n*-alkane dimers benchmark[18] set contains six dimerization energies for all–*trans*–*n*–alkane molecules from ethane to heptane (Figure 4). The CCSD(T)/CBS reference energies were MP2/CBS values corrected by the (CCSD(T) − MP2)/cc-pVTZ estimate for ethane to butane and a linear extrapolation of the coupled cluster correction (kcal/mol) by $-0.068 + 0.0616\,x$, where x is the number of carbon atoms in the monomer, for the longer chains. These reference values are listed in Table V along with the EFP2 results. Interaction energies for these complexes vary from −1.3 kcal/mol to −5.6 kcal/mol. The EFP2-CAMB3LYP-D3 interaction energies are in good agreement with the reference values in Table V. We found that EFP2 interaction energies do not vary significantly with basis sets and localization (Boys and Emiston-Ruedenberg) methods. The EFP2/CAMB3LYP potential generated with the aug-cc-pVTZ basis set has the MUE of 0.5 kcal/mol. This is much smaller than the MUE of 2.5 kcal/mol obtained with the EFP2/HF potential using the same basis set.

V. SUMMARY AND CONCLUSIONS

A method for generating effective fragment potentials based on density functional theory (EFP2-DFT) is developed for the treatment of solvent effects. EFP2-DFT includes electrostatic, exchange-repulsion, polarization, and dispersion, which are generated for a chosen DFT functional for a given isolated molecule with a computational cost comparable to that of the HF based EFP2 method. In analogy to the HF based EFP2, the electrostatic potential is modeled with multipolar expansion at each atomic center and bond midpoint by Stone′s DFT distributed multipolar analysis. The exchange–repulsion potential between two fragments is composed of the overlap and kinetic energy integrals and the nondiagonal KS matrices in the localized molecular orbital basis. The polarization potential is derived from the static molecular polarizability from DFT finite field calculations and approximate coupled perturbed Kohn-Sham equations. The dispersion potential incorporates the low cost D3 dispersion correction of Grimme *et al.*[28] that extends the range applicability of EFP to larger system sizes and provides comparable or improved results for EFP2-DFT over previous HF based EFP2 method, which has MUEs of 2.41, 3.1, 1.8, and 2.5 kcal/mol for the S22, water-benzene clusters, water clusters, and *n*-alkane dimers benchmark sets, respectively. A DFT based EFP2 potential using the CAM-B3LYP functional was evaluated with the same benchmark sets and yielded the corresponding MUEs of 1.7, 2.2, 2.0, and 0.5 kcal/mol for the respective sets.

ACKNOWLEDGMENTS

This research has been supported by the Air Force Office of Scientific Research and by CPU time from the Air Force Research Laboratory DoD Supercomputing Resource Center.

[1]M. S. Gordon, M. A. Freitag, P. Bandyopadhyay, J. H. Jensen, V. Kairys, and W. J. Stevens, J. Phys. Chem. A **105**, 293 (2001).
[2]M. S. Gordon, D. G. Fedorov, S. R. Pruitt, and L. V. Slipchenko, Chem. Rev. **112**, 632 (2012).
[3]P. N. Day, J. H. Jensen, M. S. Gordon, S. P. Webb, W. J. Stevens, M. Krauss, D. Garmer, H. Basch, and D. Cohen, J. Chem. Phys. **105**, 1968 (1996).
[4]M. S. Gordon, Q. A. Smith, P. Xu, and L. V. Slipchenko, Annu. Rev. Phys. Chem. **64**, 553 (2013).
[5]N. Gresh, G. A. Cisneros, T. A. Darden, and J.-P. Piquemal, J. Chem. Theory Comput. **3**, 1960 (2007).
[6]W. Chen and M. S. Gordon, J. Chem. Phys. **105**, 11081 (1996).
[7]A. Adamovic, M. A. Freitag, and M. S. Gordon, J. Chem. Phys. **118**, 6725 (2003).
[8]A. Adamovic and M. S. Gordon, Mol. Phys. **103**, 379 (2005).
[9]Q. A. Smith, K. Ruedenberg, M. S. Gordon, and L. V. Slipchenko, J. Chem. Phys. **136**, 244107–1 (2012).
[10]J. H. Jensen and M. S. Gordon, Mol. Phys. **89**, 1313 (1996).
[11]J. H. Jensen and M. S. Gordon, J. Chem. Phys. **108**, 4772 (1998).
[12]H. Li, M. S. Gordon, and J. H. Jensen, J. Chem. Phys. **124**, 214108–1 (2006).
[13]S. Grimme, J. Antony, S. Ehrlich, and H. Krieg, J. Chem. Phys. **132**, 154104 (2010).
[14]P. Jurecka, J. Sponer, J. Cerny, and P. Hobza, Phys. Chem. Chem. Phys. **8**, 1985 (2006).
[15]V. S. Bryantsev, M. S. Diallo, A. C. T. van Duin, and W. A. Goddard, J. Chem. Theory Comput. **5**, 1016 (2009).
[16]T. Takatani, E. G. Hohenstein, M. Malagoli, M. S. Marshall, and C. D. Sherrill, J. Chem. Phys. **132**, 144104 (2010).
[17]L. V. Slipchenko and M. S. Gordon, J. Phys. Chem. A **113**, 2092 (2009).
[18]S. Tsuzuki, K. Honda, T. Uchimaru, and M. Mikami, J. Chem. Phys. **124**, 114304 (2006).
[19]A. J. Stone, J. Chem. Theory Comput. **1**, 1128 (2005).
[20]L. V. Slipchenko and M. S. Gordon, Mol. Phys. **107**, 999 (2009).
[21]M. A. Freitag, J. H. Jensen, M. S. Gordon, and W. J. Stevens, J. Chem. Phys. **112**, 7300 (2000).
[22]B. Jeziorski, R. Moszynski, and K. Szalewicz, Chem. Rev. **94**, 1887 (1994).
[23]H. L. Williams and C. F. Chabalowski, J. Phys. Chem. A **105**, 646 (2001).

[24]A. Heßelmann and G. Jansen, Chem. Phys. Lett. **357**, 464 (2002).
[25]A. J. Misquitta and K. Szalewicz, Chem. Phys. Lett. **357**, 301 (2002).
[26]K. A. Nguyen, P. N. Day, and R. Pachter, J. Chem. Phys. **135**, 074109–1 (2011).
[27]T. Yanai, D. P. Tew, and N. C. Handy, Chem. Phys. Lett. **393**, 51 (2004).
[28]L. Goerigk and S. Grimme, Phys. Chem. Chem. Phys. **13**, 6670 (2011).
[29]D. R. Garmer and W. J. Stevens, J. Phys. Chem. **93**, 8263 (1989).
[30]J. A. Pople, R. Krishnan, B. Schlegel, and J. S. Binkley, Int. J. Quantum Chem. Symp. **13**, 325 (1979).
[31]H. Sekino and R. J. Bartlett, J. Chem. Phys. **85**, 976 (1986).
[32]J. E. Rice and N. C. Handy, J. Chem. Phys. **94**, 4959 (1991).
[33]J. G. Ángyán, G. Jansen, M. Loos, C. Hättig, and B. A. Heβ, Chem. Phys. Lett. **219**, 267 (1994).
[34]R. M. Minikis, V. Kairys, and J. H. Jensen, J. Phys. Chem. A **105**, 3829 (2001).
[35]A. M. Lee and S. M. Colwell, J. Chem. Phys. **101**, 9704 (1994).
[36]M. Kamiya, H. Sekino, T. Tsuneda, and K. Hirao, J. Chem. Phys. **122**, 234111 (2005).
[37]J. C. Flick, D. Kosenkov, E. G. Hohenstein, C. D. Sherrill, and L. V. Slipchenko, J. Chem. Theory Comput. **8**, 2835 (2012).
[38]N. B. Balabanov and K. A. Peterson, J. Chem. Phys. **123**, 064107 (2005).
[39]J. M. L. Martin and A. Sundermann, J. Chem. Phys. **114**, 3408 (2001).
[40]W. Kohn and L. J. Sham, Phys. Rev. **140**, A1133 (1965).
[41]K. A. Nguyen, P. N. Day, and P. Pacher, Int. J. Quantum Chem. **110**, 2247 (2010).
[42]G. S. Fanourgakis, E. Aprà, and S. S. Xantheas, J. Chem. Phys. **121**, 2655 (2004).
[43]M. W. Schmidt, K. K. Baldridge, J. A. Boatz, S. T. Elbert, M. S. Gordon, J. H. Jensen, S. Koseki, N. Matsunaga, K. A. Nguyen, S. Su, T. L. Windus, M. Dupuis, and J. A. Montgomery, J. Comput. Chem. **14**, 1347 (1993).
[44]See supplementary material at http://dx.doi.org/10.1063/1.4883488 for computed binding energy components for the S22 benchmark.
[45]P. N. Day, R. Pachter, M. S. Gordon, and G. N. Merrill, J. Chem. Phys. **112**, 2063 (2000).
[46]A. J. Misquitta, R. Podeszwa, B. Jeziorski, and K. Szalewicz, J. Chem. Phys. **123**, 214103 (2005).